Supporting Information

Synchronous Redox Reactions in Copper Oxalate Enable High-Capacity Anode for Proton Battery

Wanxin Song,[1] Jianyong Zhang,[1] Cheng Wen,[1] Haiyan Lu,[1] Chunhua Han,[1] Lin Xu, [1,2,3]* and Liqiang Mai[1,2,3]*

1 State Key Laboratory of Advanced Technology for Materials Synthesis and Processing, School of Materials Science and Engineering, Wuhan University of Technology, Wuhan 430070, China

2 Hubei Longzhong Laboratory, Wuhan University of Technology (Xiangyang Demonstration Zone), Xiangyang 441000, China

3 Hainan Institute, Wuhan University of Technology, Sanya 572000, China

KEYWORDS: Aqueous Battery; Proton; Copper Oxalate; Polyanion; High Capacity.

Experimental section

Materials: The following materials are commercially available: $Cu(CH_3COO)_2 \cdot H_2O$ (99.95%, metals basis), $C_2H_2O_4 \cdot 2H_2O$ (Guaranteed Reagent, 99.8%), $K_3Fe(CN)_6$ (99.95%, metals basis), $CuSO_4 \cdot 5H_2O$ (99.99%, metals basis) were purchased from Aladdin Biochemical Technology Co Ltd. Polyvinylidene fluoride (PVDF) and acetylene black were purchased from Guangdong Canrd New Energy Technology Co Ltd. And isopropyl alcohol (≥ 99.7%, Ar) was purchased from Sinopharm Chemical Reagent Co Ltd. All of the reagents were directly used without further purification.

Preparation of CuC_2O_4: The $CuC_2O_4 \cdot 0.5H_2O$ ($CuCO_x$ for short) was prepared by a simple one-step synthesis method in an aqueous solvent. Typically, 20 mL of $Cu(CH_3COO)_2 \cdot H_2O$ solution (2 mmol) was added dropwise into 80 mL of $C_2H_2O_4 \cdot 2H_2O$ solution (2 mmol) under magnetic stirring at 30 ℃. After 30 minutes of reaction, the blue precipitate was rinsed three times with deionized water and isopropyl alcohol (for quick drying), then dried overnight in a vacuum oven at 30 ℃.

Preparation of CuFe-TBA: The CuFe-TBA were synthesized according to the reference.[1] 40 mL of $CuSO_4$ solution (0.2 M) was added dropwise into 40 mL of $K_3Fe(CN)_6$ solution (0.1 M) under magnetic stirring. After six hours of reaction, the olive-green precipitate was rinsed with deionized water, centrifuged multiple times, and then dried in an oven at 60 °C overnight.

Characterization: The in-situ X-ray diffraction (XRD) patterns were probed on a monochromator Co source Kα X-ray (λ = 1.78886 Å) by the Bruker D8 Discover X-ray diffractometer. The XRD spectra of raw materials were collected by the Bruker D2

Discover X-ray diffractometer, employing Cu Kα radiation (λ = 1.5406 Å). TOPAS software was used to perform XRD refinement. SEM images were taken via a JEOL JSM-7100F in 20 kV (voltage). TEM images and EDS mapping were collected with a JEM-2100F and a Thermo Fischer Titan G2 60-300 microscope. X-ray photoelectron spectroscopy (XPS) was introduced to evaluate the valence of elements (Type: VG MultiLab 2000). Fourier Transform Infrared Spectroscopy (FTIR) was conducted on a Thermo Nicolet Nexus instrument. ESR measurement was collected with a JESFA200 instrument. The in-situ Raman patterns and ex-situ Raman spectra of electrodes were probed with 532 nm laser resources by Horiba LabRAM HR Evolution. Raman spectra of pristine materials were obtained by LabRAM Odyssey with a wavelength of 532 nm. The thermogravimetric (TG) measurements were performed on a STA449F3 at a heating rate of 5 ℃/min under an argon atmosphere.

Electrochemical measurements: The electrochemical performance of the $CuCO_x$ electrode was evaluated with a typical three-electrode system, including $CuCO_x$ as the working electrode, carbon cloth as the counter electrode, $Hg/HgSO_4$ electrode (MSE) as the reference electrode, and 0.1 M H_2SO_4 as the electrolyte. It is worth noting that the protective liquid used by the MSE is saturated K_2SO_4. In order to eliminate the adverse effect of K^+ on the electrochemical test, we replaced the protective fluid with 1 M H_2SO_4 solution. After testing (Figure S21), the voltage difference between the replaced MSE and the previous one is -0.009 V, which is much smaller than the standard electrode potential of MSE (0.64 V vs SHE), so it can be ignored. The OCV test reveals that the voltage difference between the two electrodes does not float more

than ± 0.5 mV. The protective fluid 1 M H_2SO_4 in the reference electrode has negligible penetration that would not affect the electrolyte concentration, as the bottom of the reference electrode is made of porous ceramic material, which serves as a barrier to penetration. To verify this conjecture, the pH values were separately measured. The results show that the initial pH value of the electrolyte is 1.21 and it is 1.20 after 80 hours of being connected with the reference electrode. Given the ±0.1 error range of the pH measuring agent, these results indicate that the concentration of the electrolyte remains unaffected. The working electrode was prepared by adding CDD carbon cloth before the stirring step of $CuCO_x$ synthesis. The mass loading of activated materials in the working electrode was 1.2 mg cm^{-2}. As for the electrochemical property measurements of the full battery, the cathode material was fabricated by mixing CuFe-TBA, acetylene black and polyvinylidene fluoride (PVDF) at a weight ratio of 7: 2: 1. The mixture was mixed with 1-methyl-2-pyrrolidone to form a slurry, then evenly coated on the titanium foil collector to obtain the cathode. The Swagelok cell used consists of two titanium rods and a polytetrafluoroethylene shell. Compared with a conventional three-electrode cell, this Swagelok cell tightly presses the anode and cathode together through two titanium rods during battery measurements, helping to prevent volatilization of the electrolyte and reduce the concentration polarization effect.[2] Cyclic voltammetry (CV) and linear sweep voltammetry (LSV) were performed on a Biologic VMP electrochemical workstation. The galvanostatic charge-discharge (GCD) performance and rate performance were conducted on a Land CT3001A battery test system (Wuhan, China).

Supporting Figures

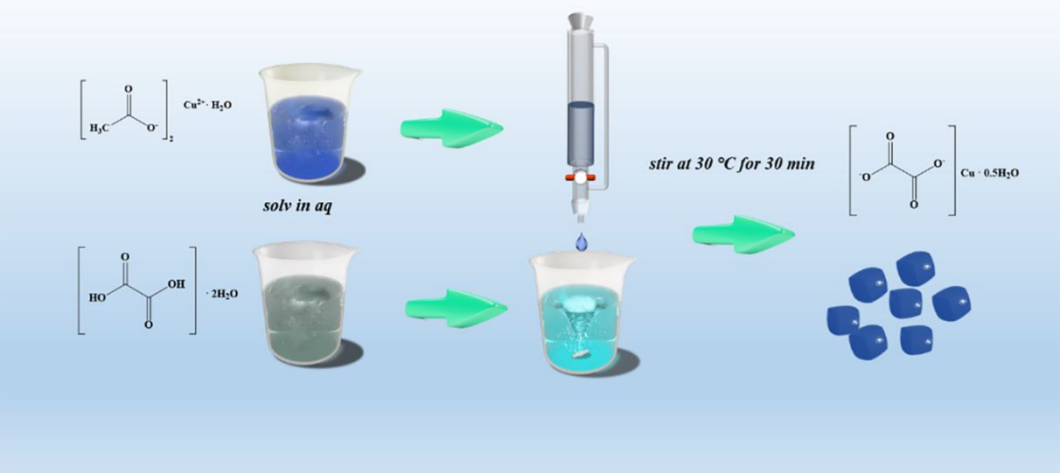

Figure S1. Synthetic process of the $CuC_2O_4 \cdot 0.5H_2O$ ($CuCO_x$ for short). It is worth noting that the one-step method in this aqueous solvent cannot strictly limit the size of the particles. After 30 minutes of stirring, the obtained copper oxalate particle size is mostly 1 micron, while there is also a small amount of less than 500 nm. However, this does not affect the performance of the $CuCO_x$, because subsequent tests show that the energy storage mechanism of copper oxalate does not involve surface effect and size effect.

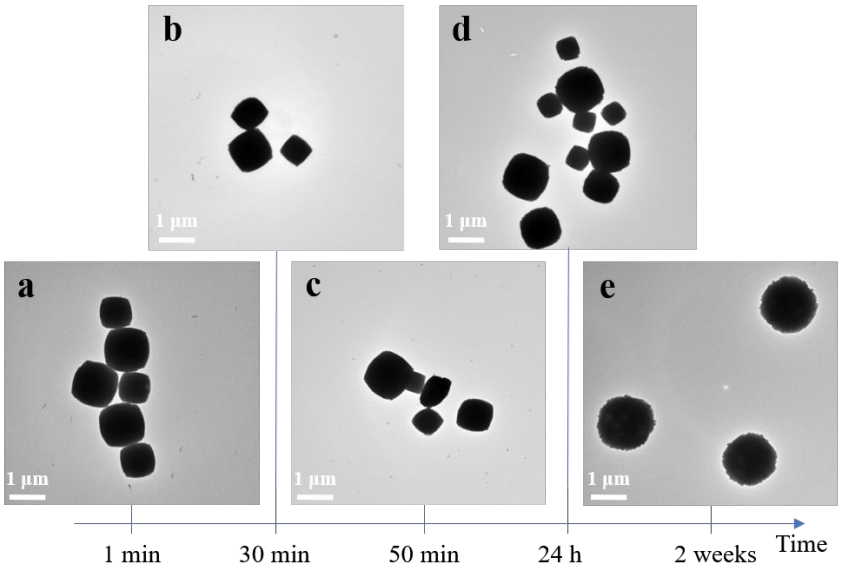

Figure S2. SEM images of $CuCO_x$ supracrystals after different precipitation times. a) 1 min, b) 30 min, c) 50 min, d) 24 h, and e) 2 weeks.

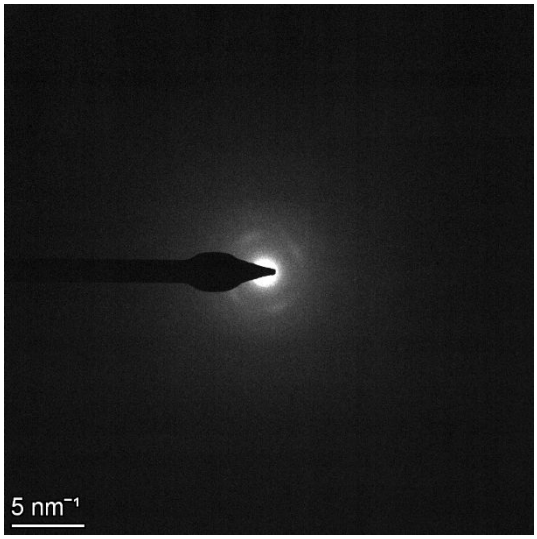

Figure S3. The electron diffraction pattern of $CuCO_x$. It is converted to an amorphous state when bombarded by high-energy electron beams.

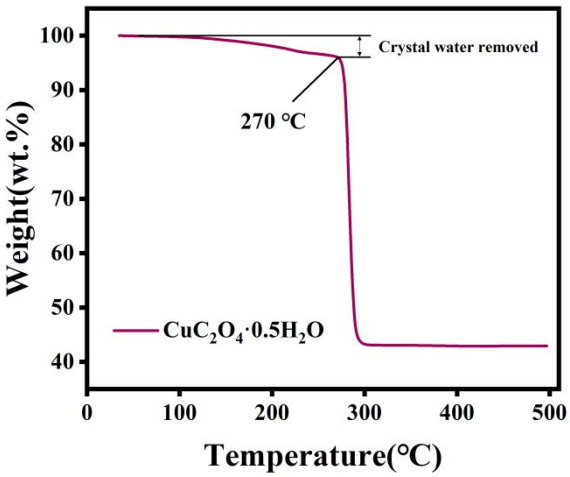

Figure S4. TGA curve of $CuCO_x$ power under argon atmosphere.

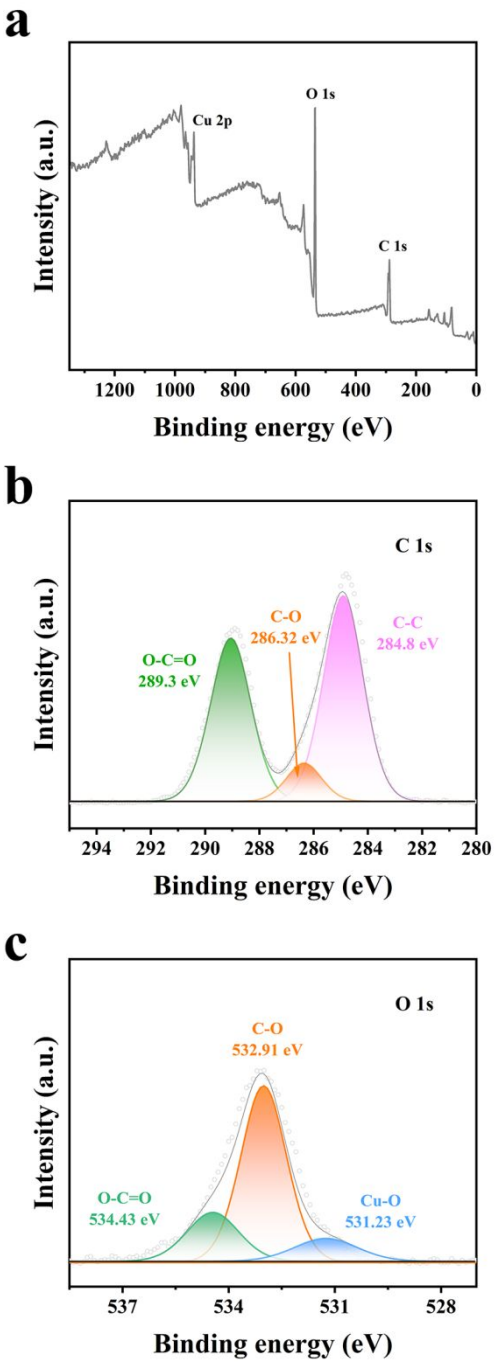

Figure S5. XPS spectra of a) $CuCO_x$, b) C 1s, and c) O 1s.

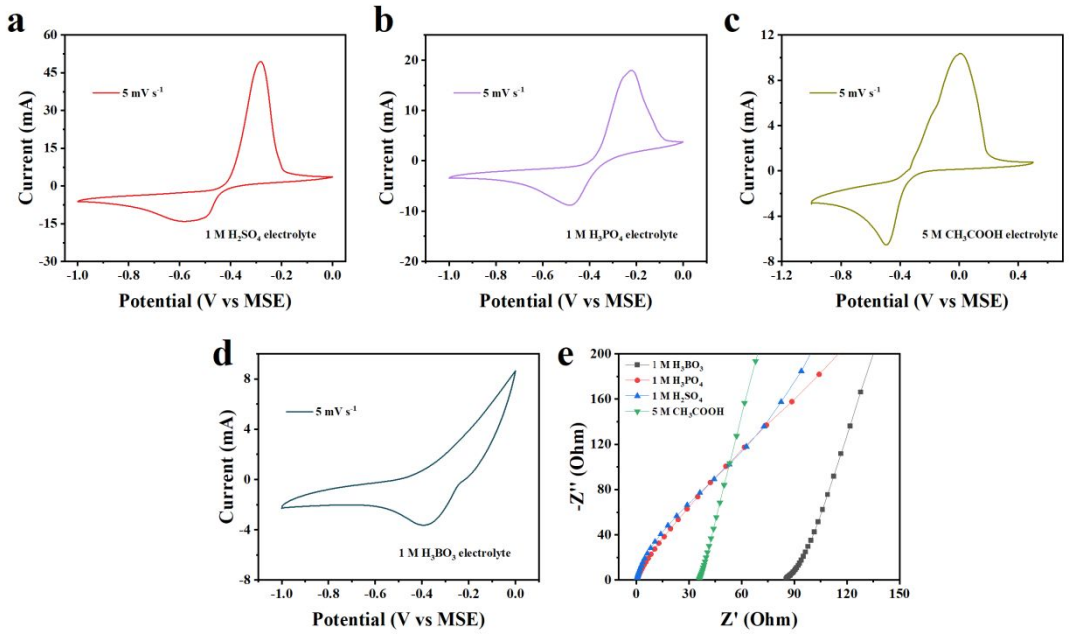

Figure S6. Comparison of different electrolytes. The CV curves of $CuCO_x$ electrode at 5 mV s^{-1} in a) 1 M H_2SO_4, b) 1 M H_3PO_4, c) 5 M CH_3COOH, and d) 1 M H_3BO_3. e) EIS measurement of these electrolytes.

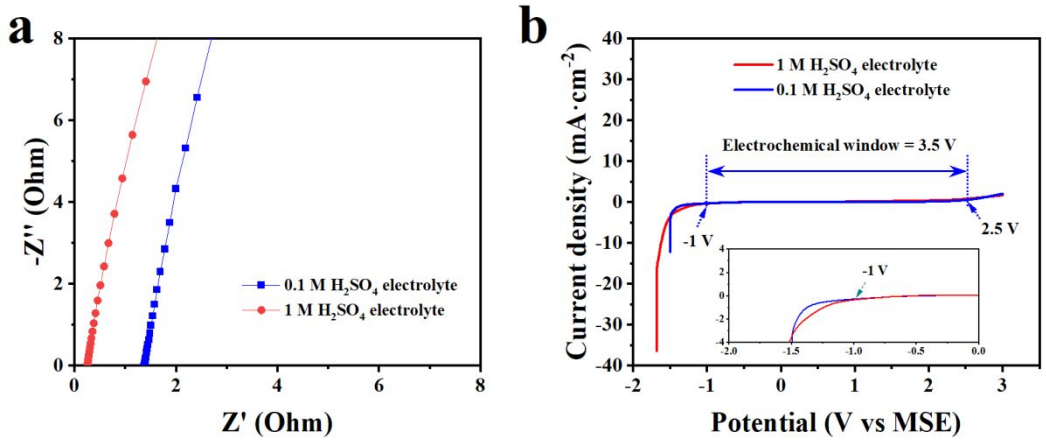

Figure S7. Comparison of the 0.1 M H_2SO_4 and 1 M H_2SO_4 electrolyte. a) EIS test, and b) electrochemical window measured by LSV at 5 $mV \cdot s^{-1}$.

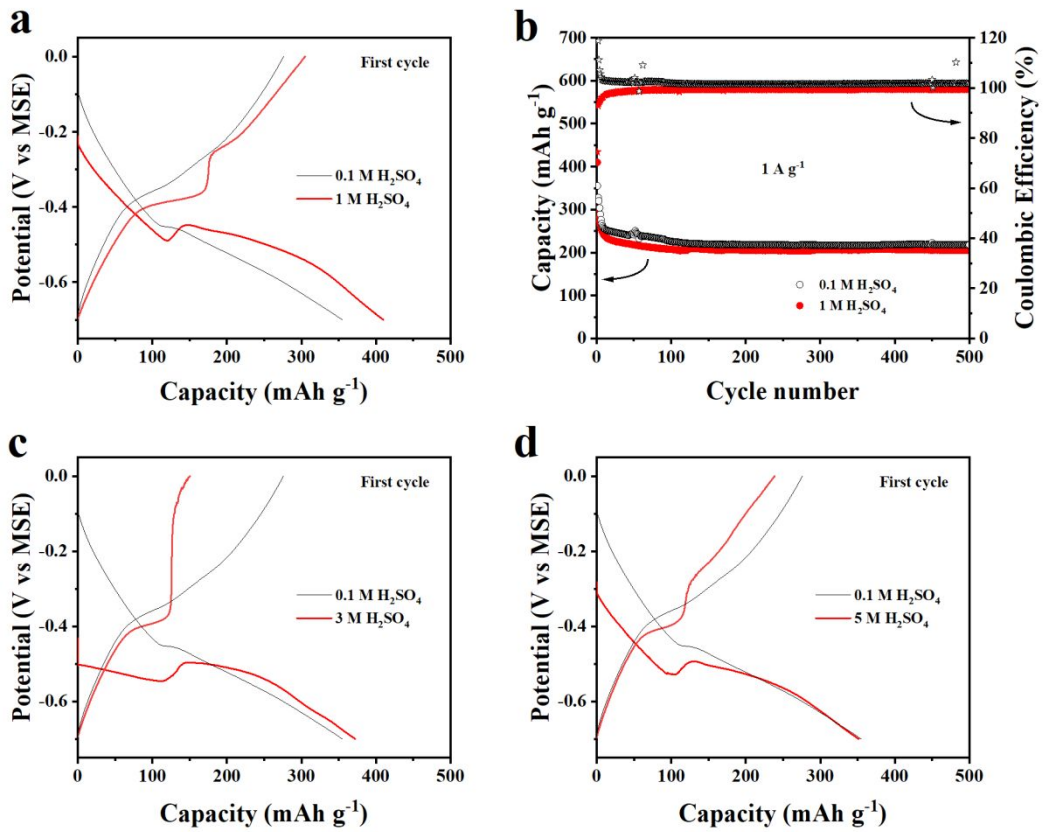

Figure S8. Electrochemical performance of $CuCO_x$ in various concentrations of H_2SO_4 electrolytes. a) GCD curves in 0.1 M/1 M H_2SO_4. b) Cycling performance in 0.1 M/1 M H_2SO_4 at 1 A g^{-1}. c-d) GCD curves in 0.1 M/3 M/5 M H_2SO_4.

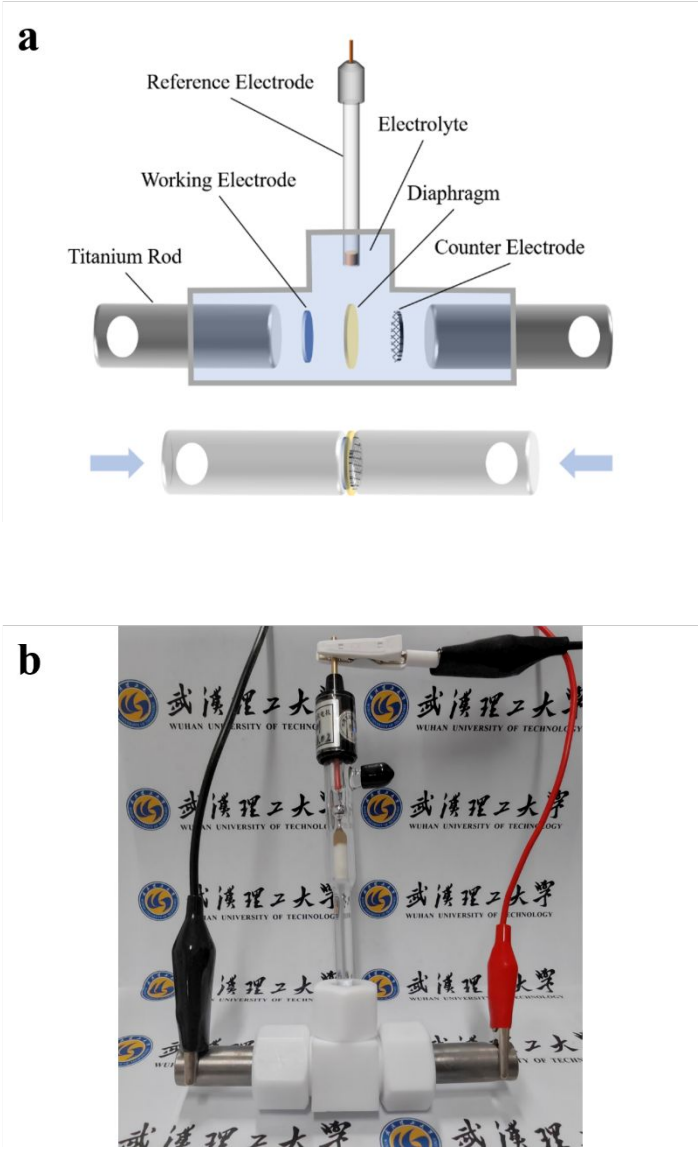

Figure S9. Structure of the Swagelok three-electrode cell. a) Detailed structure of the model. b) A scene photograph of three-electrode during testing.

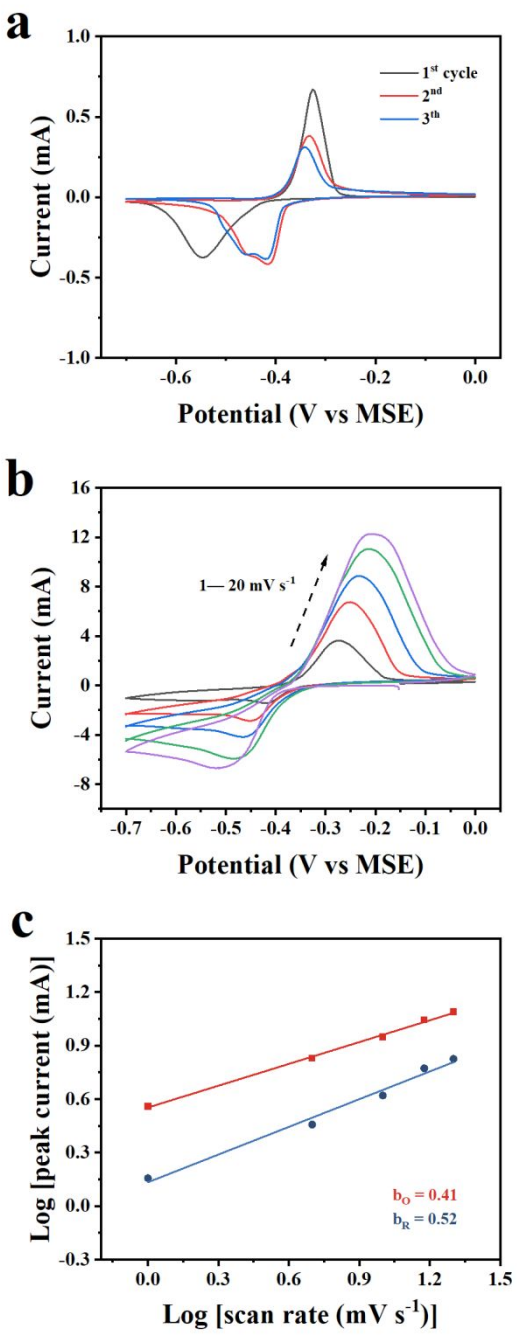

Figure S10. Three-electrode electrochemical test of $CuCO_x$ electrode on titanium foil collector. a) Typical CV curves for the initial three cycles at a scan rate of 0.1 mV s^{-1}. b) CV curves at various scan rates between 1 – 20 mVs^{-1}. c) The corresponding plots of log (peak current) vs. log (scan rate) according to the CV curves.

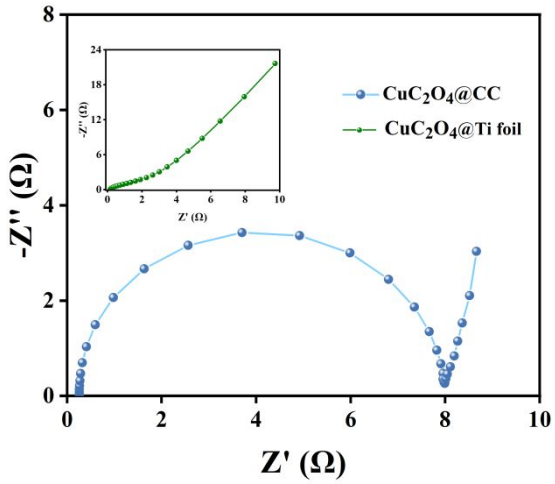

Figure S11. Nyquist plots obtained from electrochemical impedance spectroscopy measurements of $CuCO_x$ electrode at 25℃.

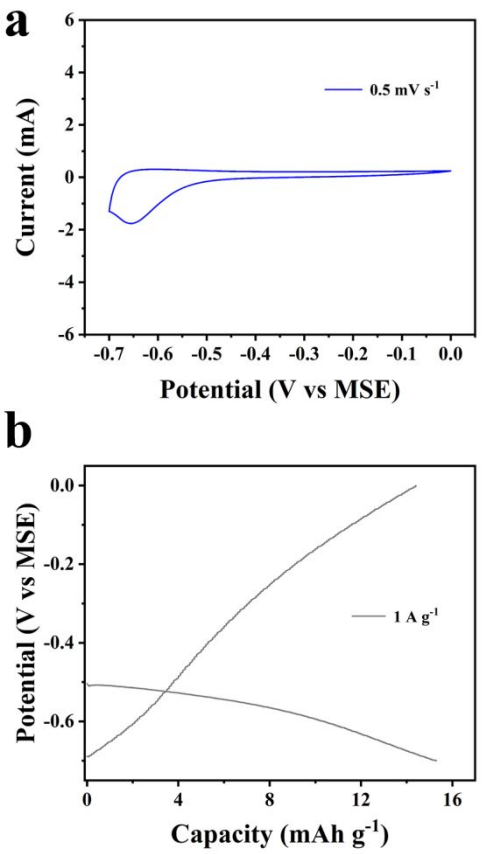

Figure S12. Electrochemical measurements for pure carbon cloth: a) CV curve at 0.5 mV s^{-1}, and b) GCD curve at 1 A g^{-1} (calculated according to the mass of active substance of $CuCO_x$).

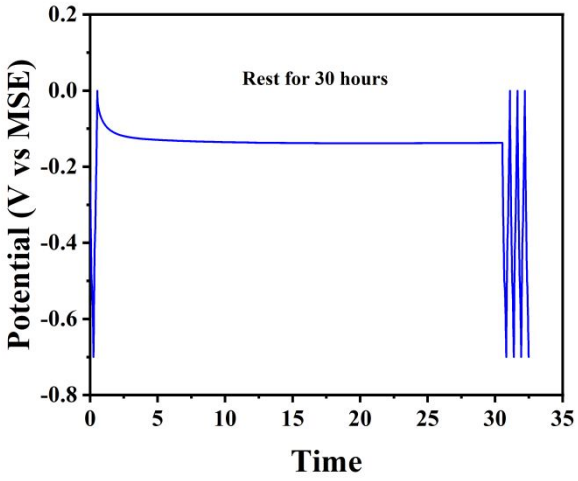

Figure S13. Time-potential profiles at 1 A g^{-1}, where the $CuCO_x$ half-cell was rested for 30 hours.

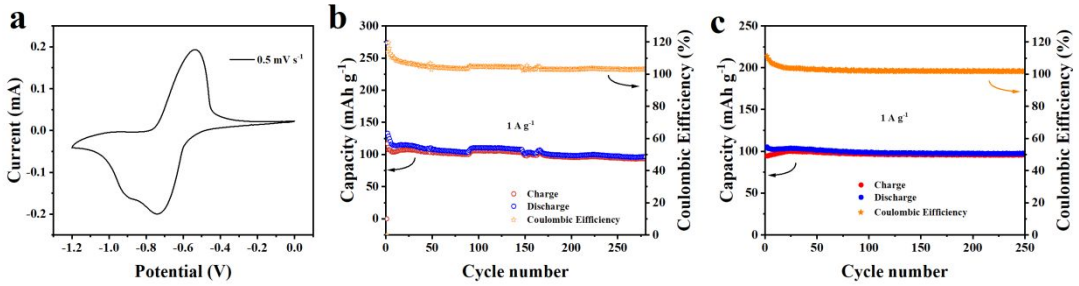

Figure S14. Electrochemical test of $CuCO_x$ electrode. a) CV curve at 0.5 mV s^{-1}, and b) cycling performance at 1 A g^{-1} in a typical two-electrode system. c) Cycling performance at 1 A g^{-1} in a cion cell.

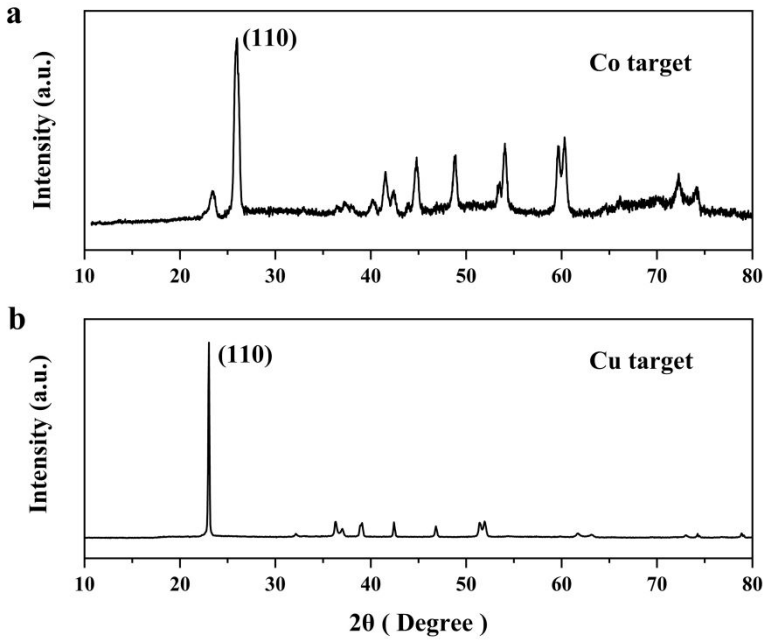

Figure 15. XRD patterns of $CuCO_x$ were obtained from a) the Co target and b) the Cu target.

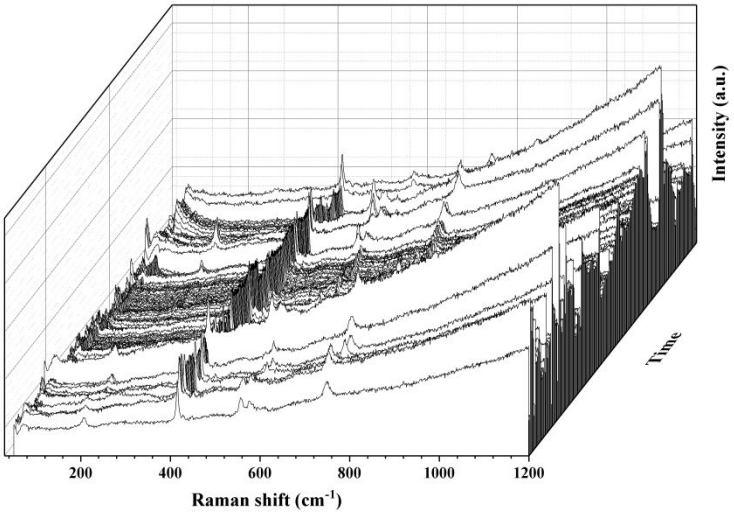

Figure S16. In-situ Raman pattern of $CuCO_x$ electrode at Raman shift from 30 to 1200 cm^{-1}, and there are severe fluorescence effects at the higher wavenumber.

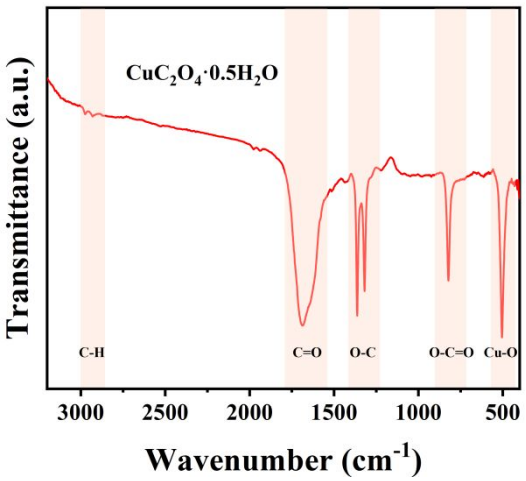

Figure S17. FTIR spectrum of $CuCO_x$ powder.

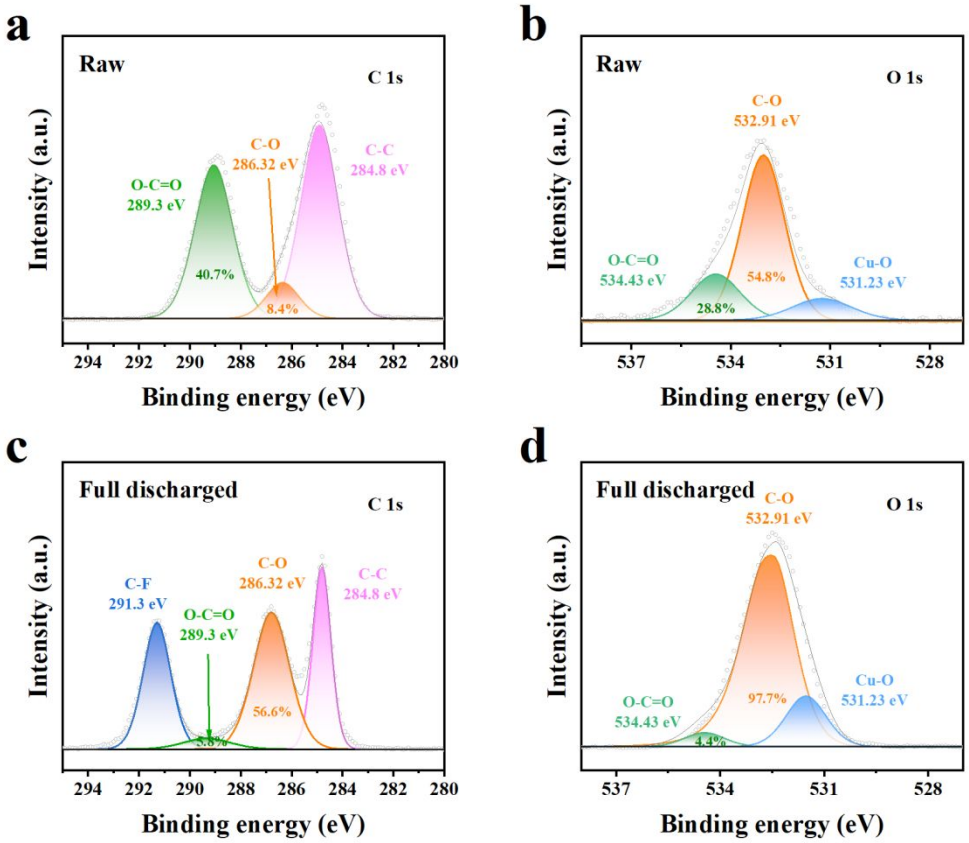

Figure S18. Ex-situ XPS spectra of $CuCO_x$ electrode at original state a) C 1s, b) O 1s and full discharged state c) C 1s, d) O 1s.

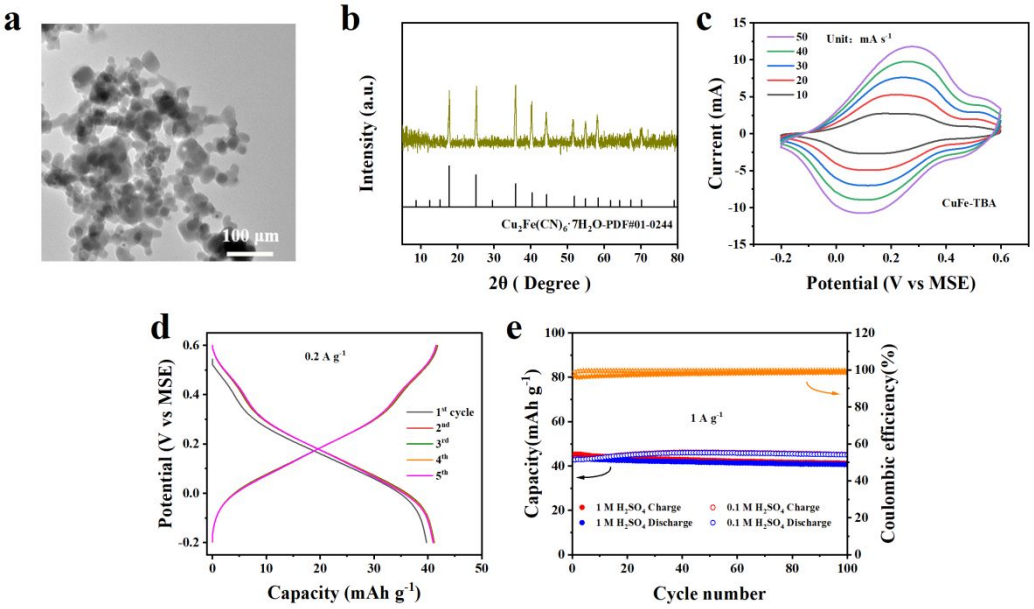

Figure S19. Characterizations and electrochemical measurements of CuFe-TBA cathode. a) TEM image, b) XRD pattern compared with PDF#01-0244, c) CV curves at various scan rates from 10 to 50 mV s^{-1}, d) GCD curves of the first five cycles, and e) cycling performance in 0.1 M /1 M H_2SO_4 electrolyte.

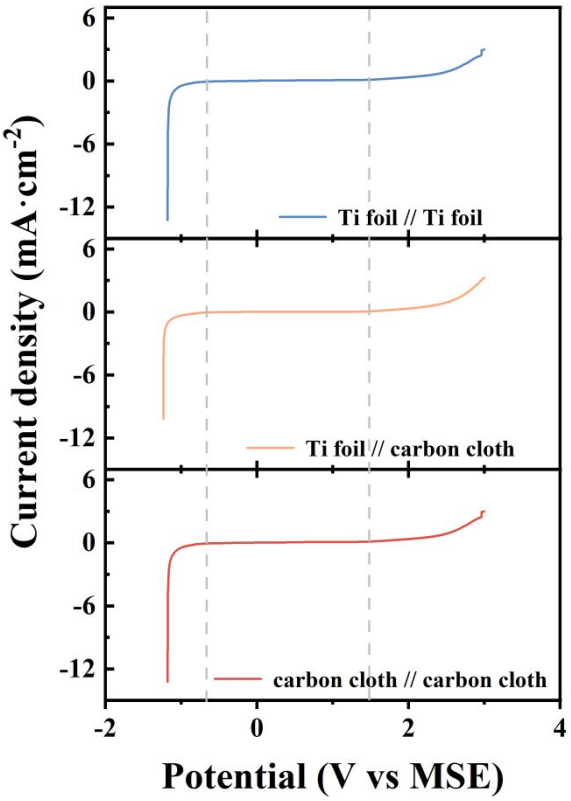

Figure S20. The LSV curves to detect the feasibility electrochemical stability window for the full cell.

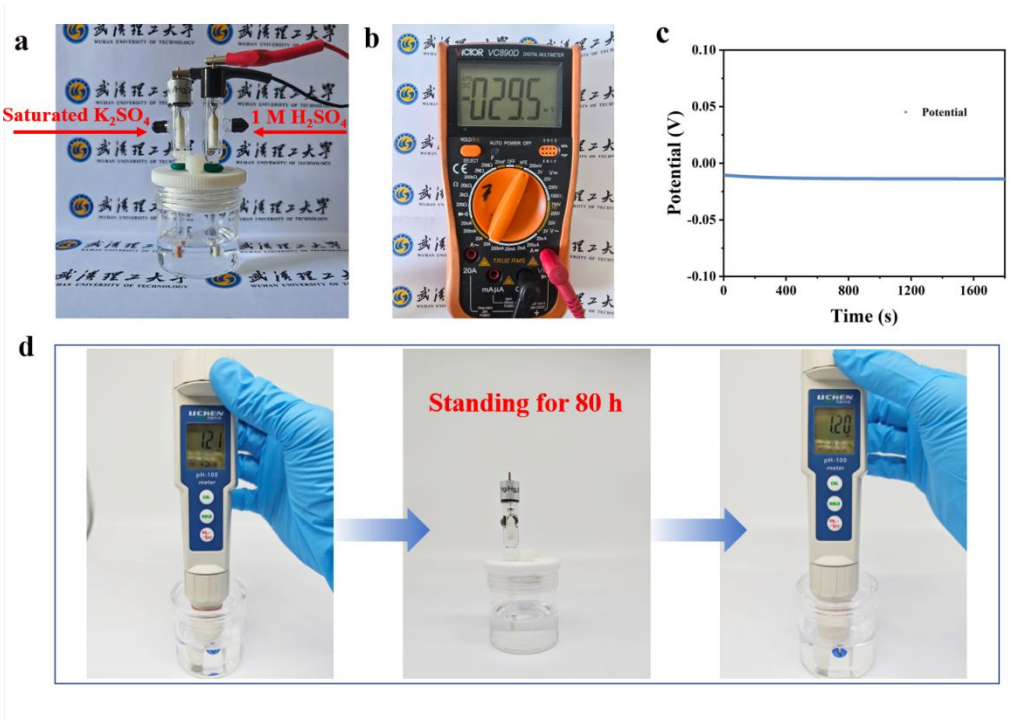

Figure S21. a) Scene photograph of two MSE reference electrodes with different protective fluids in 0.1 M H_2SO_4 electrolyte. b) The voltage difference (0.009 V) between two MSE electrodes. c) The open circuit voltage (OCV) curve of two electrodes. d) PH values of the electrolyte before and after connecting with the reference electrode.

References

(1) Wu, X.; Hong, J. J.; Shin, W.; Ma, L.; Liu, T.; Bi, X.; Yuan, Y.; Qi, Y.; Surta, T. W.; Huang, W.; Neuefeind, J.; Wu, T.; Greaney, P. A.; Lu, J.; Ji, X., Diffusion-free Grotthuss topochemistry for high-rate and long-life proton batteries. *Nat. Energy* **2019,** *4* (2), 123-130.

(2) Wang, C.; Zhao, S.; Song, X.; Wang, N.; Peng, H.; Su, J.; Zeng, S.; Xu, X.; Yang, J., Suppressed Dissolution and Enhanced Desolvation in Core–Shell MoO_3@TiO_2 Nanorods as a High-Rate and Long-Life Anode Material for Proton Batteries. *Adv. Energy Mater.* **2022**, 2200157.